Frontiers of Information Technology & Electronic Engineering
www.jzus.zju.edu.cn; engineering.cae.cn; www.springerlink.com
ISSN 2095-9184 (print); ISSN 2095-9230 (online)
E-mail: jzus@zju.edu.cn

Correspondence:

Simultaneous wireless information and power transmission system based on a dual-frequency metasurface design*

Yicen LI, Mingyang CHANG, Hao XUE, Haixia LIU, Long LI†‡

School of Electronic Engineering, Xidian University, Xi'an 710071, China

†E-mail: lilong@mail.xidian.edu.cn

Received Apr. 30, 2024; Revision accepted Oct. 4, 2024; Crosschecked Nov. 25, 2024

https://doi.org/10.1631/FITEE.2400345

Nowadays, the number of wireless sensor devices is increasing rapidly, posing persistent challenges related to battery replacement and power wiring. This paper presents a simultaneous wireless information and power transmission (SWIPT) scheme based on a frequency diversity metasurface design, which provides a wireless power supply scheme for electrical devices such as sensors. The metasurface is designed with frequency bands commonly found in the environment, and achieves efficient absorption of electromagnetic (EM) energy at 5.8 GHz and radiation of sensor information at 2.45 GHz, making it possible to take full advantage of the energy in the environment and easy to integrate with existing systems. The branches for the dual-square loop are designed based on spatial impedance matching and equivalent circuit, giving the metasurface advantages such as compact layout (unit size of $0.16\lambda_0\times0.16\lambda_0\times0.012\lambda_0$, where λ_0 is the wavelength at 2.45 GHz), high isolation ($S_{21}<-20$ dB within the operating frequency band), and insensitivity to incident angles (efficiency over 80% within 60°). Integrated with rectification circuits and sensors, it efficiently converts EM waves received by the metasurface into direct current (DC) power for sensor operation. The sensors then radiate information through the metasurface, effectively addressing challenges related to sensor device wiring and battery replacement, thereby offering new solutions for the development of next-generation smart cities.

1 Introduction

Since the start of the 21st century, wireless communication technology (WCT) and the Internet of Things (IoT) have experienced rapid development, leading to the continuous expansion of wireless communication. This growth has been accompanied by a geometric increase in electronic devices, particularly in the case of implantable medical devices for humans and tens of thousands of miniaturized and low-power wireless sensors (Shibata et al., 2001; Cheng et al., 2013; Bakogianni and Koulouridis, 2016; Li et al., 2018). However, there are still some challenges such as wiring difficulties and the high cost of battery replacement in these devices (Xue et al., 2024). The emergence of the SWIPT technology (Mohsan et al., 2023) allows for energy provision to communication devices while exchanging information, thereby overcoming the limitations of traditional batteries and wired connections. It provides a new approach

‡ Corresponding author

* Project supported by the National Key Research and Development Program of China (No. 2023YFB3811503), the National Natural Science Foundation of China (No. 62288101), the Key Research and Development Program of Shaanxi Province, China (No. 2021TD-07), and the Fundamental Research Funds for the Central Universities, China (No. 20103224952)

ORCID: Yicen LI, https://orcid.org/0009-0004-5263-0845; Mingyang CHANG, https://orcid.org/0000-0002-2790-4638; Hao XUE, https://orcid.org/0009-0001-6234-7208; Haixia LIU, https://orcid.org/0000-0003-2610-5751; Long LI, https://orcid.org/0000-0003-0472-7314

to supplying power for sensors, enabling electronic devices to break free from the constraints of batteries and power lines, thereby extending their lifespan (Piñuela et al., 2013; Andrews et al., 2014; Fang et al., 2015; Wang X et al., 2023; Liu et al., 2024).

In SWIPT systems, the current mainstream methods include frequency diversity and polarization diversity. For frequency diversity, a dual-channel frequency-reconfigurable antenna for the SWIPT system was designed (Lu et al., 2017). A planar dipole antenna was used as the receiving antenna and defect ground structures were introduced to enhance isolation between the two ports, achieving efficient SWIPT for different scenarios. A dual-band wearable antenna was designed using conductive textiles (Wagih et al., 2021). Coupled feeding was used as a square patch to generate resonance at 2.4 GHz with a gain of 7.2 dBi for Wi-Fi communication, while the planar dipole was successfully miniaturized through bending and integration with the patch, achieving resonance for energy harvesting in the lower frequency band (785–875 MHz). For polarization diversity, a dual-polarization rectenna for the SWIPT system was proposed (Yang et al., 2013). By using slot-coupled feeding, the patch antenna achieved dual polarization at 5.8 GHz, with high isolation between ports, using the characteristics of polarization diversity to achieve synergistic energy and information transmission. A two-orthogonally-polarized Huygens line antenna was designed to form a dual-polarization antenna (Lin and Ziolkowski, 2019). Similarly, leveraging polarization diversity, they achieved energy harvesting communication in the 915 MHz industrial, scientific, and medical (ISM) frequency band and realized antenna miniaturization and high port isolation of 30 dB through a tightly coupled feeding design.

The SWIPT system has grown by leaps and bounds in recent years, due to the subwavelength unit cells of metasurfaces. These typically exhibit compact, miniaturized, and rotationally symmetrical structural characteristics and have advantages such as polarization insensitivity and wide-angle incidence. Consequently, significant research effort is being applied to metasurfaces for the design of radio frequency (RF) energy harvesting devices (Zhong et al., 2016; Zhang et al., 2017; El Badawe and Ramahi, 2018; Yu et al., 2018; Erkmen and Ramahi, 2021; Wang CC et al., 2022). A compact and polarization-insensitive rectenna based on a metasurface was designed at a frequency of 5.8 GHz (Chang et al., 2024). A multi-frequency and multi-mode metasurface was also designed for efficient RF and microwave energy harvesting (Huang et al., 2023). A novel rectifying metasurface with high efficiency was designed for use in low power scenarios (Lee and Hong, 2020). A polarization-independent dual-band metasurface absorber based on an improved Minkowski fractal structure was proposed for wireless power transmission (Gao et al., 2023).

These designs achieve efficient absorption of EM energy but require miniaturization and high port isolation to reduce interference with information during energy transmission, which is applied in the SWIPT system. Traditional rectifier antennas often require complex feeding networks to achieve dual polarization or high port isolation. This complexity not only increases energy loss but also enlarges the array during design. To address these challenges, we present a dual-frequency metasurface designed for SWIPT systems (Fig. 1). The proposed system uses frequency diversity to enable efficient energy harvesting and transmission within a more compact form, using two commonly used frequency bands, 5.8 GHz for RF–DC conversion and 2.45 GHz for sensor data transmission. The metasurface structure is engineered to efficiently absorb EM energy, ensuring high port isolation with a smaller size. Additionally, integrated sensors enable the self-powering of small appliances, effectively eliminating the need for regular battery replacement.

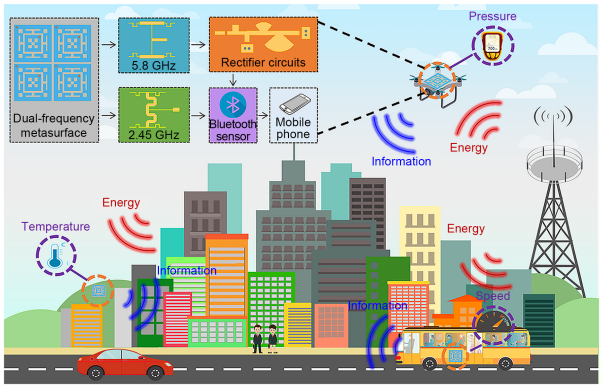

Fig. 1 System operation principle diagram

2 Theory and methods

Here, we present the theory and methods for producing high-performance dual-frequency metasurfaces.

2.1 Design of the metasurface unit

The design process of the unit is shown in Fig. 2. The metasurface unit consists of a radiating and receiving common-aperture structure on the surface, an S7136H dielectric substrate (dielectric constant=3.55, loss tangent=0.0039) in the middle, and a metal ground at the bottom.

To realize the dual-frequency metasurface with a smaller size, the design process of the unit structure is illustrated below. First, we use a dual-square loop design to realize the two frequencies: the outer loop operating at low frequency and the inner loop operating at high frequency (Fig. 2a). Second, to achieve miniaturization, branches are added to the dual-square loop to extend the current path (Fig. 2b). However, due to the limited spacing between the dual-square loops, it is not feasible to add long branches to the inner loop for miniaturization. The two branches are added to the outer loop to further achieve miniaturization at low frequency because of the larger wavelength at 2.45 GHz than at 5.8 GHz (Fig. 2c). Finally, the length of the two branches is extended to operate at 2.45 GHz (Fig. 2d).

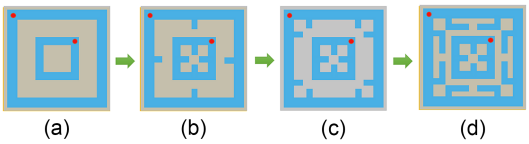

Fig. 2 Process of unit design: (a) dual-square loop design; (b) branches added to the dual-square loop; (c) further miniaturization design; (d) the proposed unit design

Simulations are conducted using ANSYS software to observe the impact of the design process on the unit frequency (Fig. 3). The designed unit is placed in an air box with a periodic boundary, along with Floquet ports to simulate the unit performance parameters. The two Floquet ports at the top and bottom are designated port f1 and port f2, respectively, while the feeding ports on the unit are designated port 1 and port 2. For the lower frequency, the unit shows a simulated S_{11} of −9.18 dB at 2.63 GHz in step 1, −21.28 dB at 2.57 GHz in step 2, −20.07 dB at 2.55 GHz in step 3, and −16.21 dB at 2.45 GHz in step 4. For the higher frequency, the unit shows a simulated S_{11} of −13.33 dB at 6.1 GHz in step 1 and −18.98 dB at 5.7 GHz in step 2. With the increase of the number of

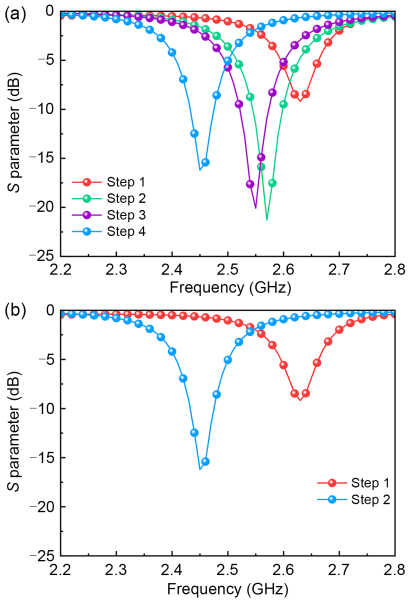

Fig. 3 Effect of the unit structure on parameters: (a) outer loop; (b) inner loop. References to color refer to the online version of this figure

branches, the current path increases, the frequency shifts lower, and finally the two required operating bands are achieved.

Compared with a rectified antenna, the metasurface design needs to consider not only the impedance matching of the loads but also the matching of the intrinsic impedance Z of the metasurface with the free space Z_0 when performing energy reception. Therefore, the metasurface structure can be adjusted to improve energy reception efficiency. The intrinsic impedance of the metasurface can be denoted as (Fante and McCormack, 1988)

$$Z=\sqrt{\frac{\mu}{\varepsilon}}=\sqrt{\frac{\mu_0}{\varepsilon_0}}\sqrt{\frac{\mu_r}{\varepsilon_r}}=Z_0\sqrt{\frac{\mu_r}{\varepsilon_r}}, \tag{1}$$

where $\mu_0=4\pi\times10^{-7}$ H/m represents the vacuum permeability, $\varepsilon_0=8.854\times10^{-12}$ F/m represents the vacuum dielectric constant, μ_r and ε_r represent the relative permeability and relative permittivity of the metasurface, respectively, and $Z_0=120\pi$ represents the intrinsic impedance of free space. When the EM wave is incident on the metasurface, the reflection coefficient Γ can be expressed as

$$\Gamma=\frac{Z-Z_0}{Z+Z_0}=\frac{\sqrt{\mu_r/\varepsilon_r}-1}{\sqrt{\mu_r/\varepsilon_r}+1}. \tag{2}$$

To achieve higher absorption efficiency, Γ must be close to zero, which means the relative permeability of the metasurface is equal to its relative permittivity: $\mu_r=\mu_r'-j\mu_r''=\varepsilon_r'-j\varepsilon_r''$.

The equivalent circuit is used to analyze the influence of the dual-square-loop structure on absorption efficiency (Fig. 4). R_{L1} and R_{L2} represent the terminal loads, R_1 represents the metal and medium loss, L_3 represents the inductance between the metal of the top and bottom layers, and the inner and outer loops can be equivalent to a separate LC resonant circuit, which are parallel. Langley and Parker (1983) have already provided a detailed derivation of relevant parameters.

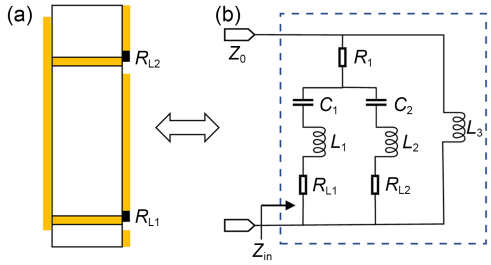

Fig. 4 Side view (a) and equivalent circuit (b) of the unit

Therefore, according to the equivalent circuit, the impedance of the unit can be expressed as

$$Z_1=\frac{1}{j\omega C_1}+j\omega L_1+R_{L1}, \tag{3}$$

$$Z_2=\frac{1}{j\omega C_2}+j\omega L_2+R_{L2}, \tag{4}$$

$$Z=(R_1+Z_1\|Z_2)\|(j\omega L_3), \tag{5}$$

where j represents the imaginary unit and ω represents the angular frequency.

Based on the above analysis, there are two ways of adjusting the EM absorption efficiency: (1) adjusting the unit structure to affect the equivalent capacitive inductance value, using adjusted unit impedance for matching with the spatial impedance (Figs. 5a–5d); (2) adjusting the terminal load to match the unit impedance with the spatial impedance (Figs. 5e and 5f). Note that because the unit structure is equivalent to LC resonant circuits, both the impedance and the resonant frequency will change when adjusting the unit structure.

The effect of the branches on the unit is analyzed (Fig. 6). By decreasing s and increasing l_3, the lower frequency of the unit can be effectively shifted lower (Figs. 6a and 6b). By increasing the length and width of the inner branches, the higher frequency of the unit can be effectively shifted lower (Figs. 6c and 6d). Note that due to the introduction of the branches, the impedance of the unit will also be affected. Therefore, we can flexibly adjust the relevant parameters of the branches on the inner and outer loops to realize the requirements for the unit frequency.

After completing the above analysis of the unit structure, the unit meets the requirements. Its structure is shown in Fig. 7. The relevant parameters are as follows: p=20 mm, l_1=18 mm, l_2=9.3 mm, l_3=8.4 mm, l_4=2 mm, w_1=4.2 mm, w_2=3.5 mm, s=0.9 mm, m_1=0.9 mm, h=1.524 mm. The top common aperture structure adopts a dual-square loop with branches suitable for two frequency bands. The unit cell size, p=20 mm, is smaller than half a wavelength, effectively addressing the issue of half-wavelength spacing between elements in traditional antennas. The impedance at both feeding ports is set to 750 Ω for load matching. The feeding ports are located at the two diagonals of the loops, with port 1 placed at the outer ring for information transmission and port 2 placed at the inner ring for energy transmission. The radius of the metalized via holes is 0.25 mm. The calculation of energy harvesting efficiency, taking port f1 as an example, is as follows:

$$A=\frac{P_L}{P_t}=1-|S_{f1f1}|^2, \tag{6}$$

where P_L represents the amount of energy received by the load and P_t represents the total transmitted power. Therefore, the energy received at port 1 of the unit is the total transmitted energy minus the energy returned to the transmitting port.

The performance of the unit is analyzed (Fig. 8). Ports 1 and 2 have reflection coefficients below −10 dB within the frequency bands of 2.41–2.49 GHz and 5.71–5.85 GHz, reaching below −25 dB at 2.45 GHz and 5.8 GHz.

Through the above analysis, the energy harvesting efficiency calculated by Eq. (6) yields the efficiency. The unit shows high energy harvesting efficiency in frequency bands. To validate the unit's wide-angle energy harvesting characteristics, the elevation angle of

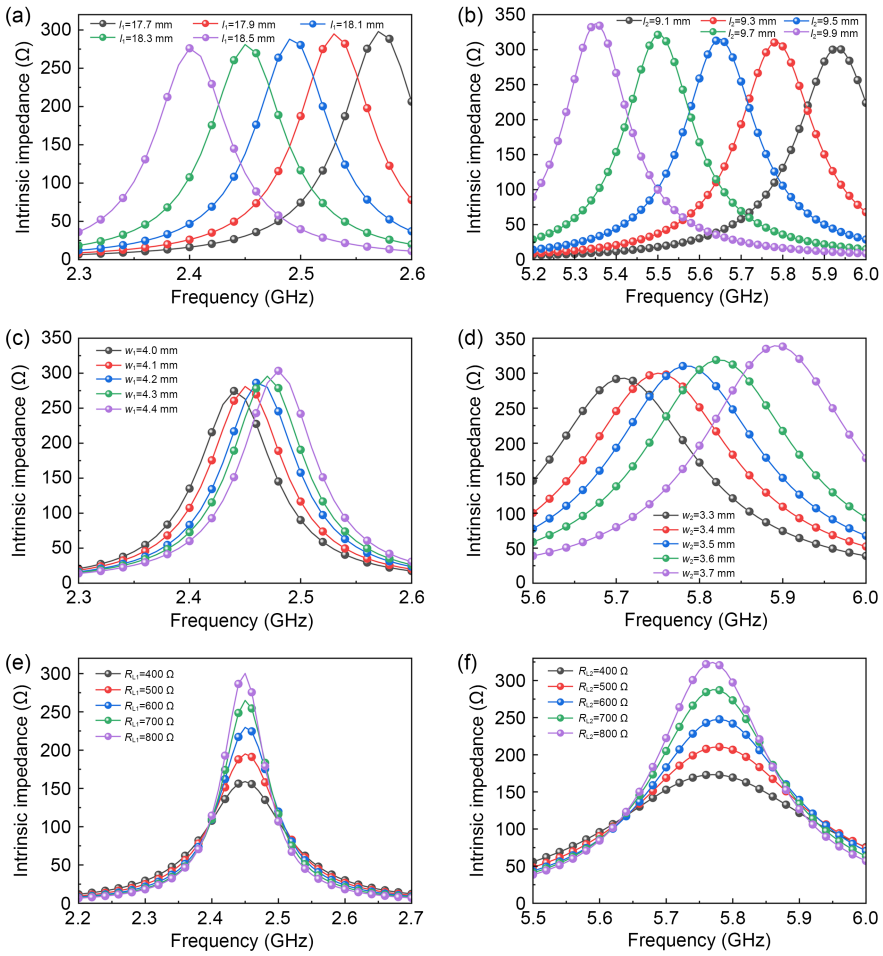

Fig. 5 Effect of unit l_1 at 2.45 GHz (a), l_2 at 5.8 GHz (b), w_1 at 2.45 GHz (c), w_2 at 5.8 GHz (d), R_{L1} at 2.45 GHz (e), and R_{L2} at 5.8 GHz (f) on intrinsic impedance. References to color refer to the online version of this figure

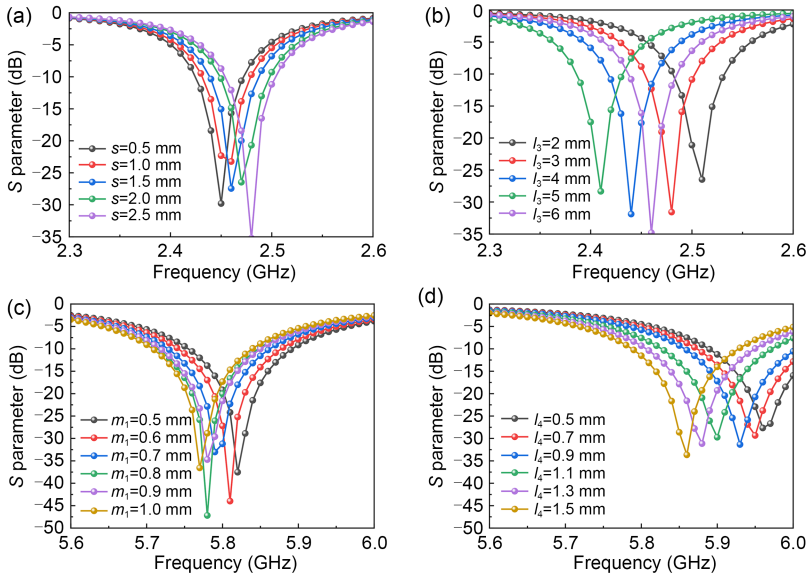

Fig. 6 Parameter scan of inner and outer branches: (a) impact of s at 2.45 GHz; (b) impact of l_3 at 2.45 GHz; (c) impact of m_1 at 5.8 GHz; (d) impact of l_4 at 5.8 GHz. References to color refer to the online version of this figure

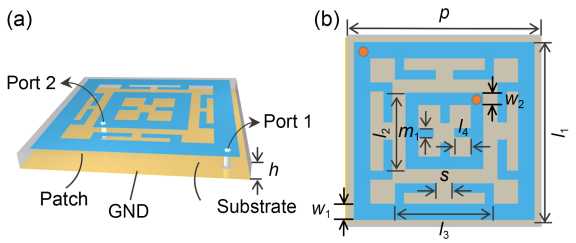

Fig. 7 Layout of the metasurface: (a) stereo view; (b) top view

the incident wave is varied, and the energy harvesting efficiency changes with the incident angle (Figs. 8c and 8d). With increasing elevation angles, there is a slight frequency offset in the peak efficiency, and the peak efficiency also decreases. However, within 60°, the energy harvesting efficiency at 2.45 GHz and 5.8 GHz remains above 80%, which shows that the designed unit structure has the ability to collect EM energy from space at wide angles.

To better understand the operation of the two unit frequencies, we analyze the electric field distribution of the dual-square loop in different bands obtained under incident wave absorption (Fig. 9). The outer loop and the added outer branches are involved mainly at 2.45 GHz, and the inner loop and the added inner branches play a major role at 5.8 GHz, showing that the added branches can effectively achieve miniaturization. The dual-square loops have little effect on each other in the two working bands, which verifies the high isolation of the unit.

2.2 Design of the metasurface array

In this subsection, a 2×2 array is designed to validate the performance (Fig. 10). A layer of dielectric substrate is added below the metasurface, and two 4-to-1 power combiners are used to combine the four ports at 5.8 GHz and 2.45 GHz into one port each. To facilitate the lamination of the two layers of dielectric substrates and the integration of rectifier circuits, the array is expanded from 40 mm×40 mm to 50 mm×50 mm. The dielectric substrate for the power combiners uses S7136H, with a thickness of 0.762 mm.

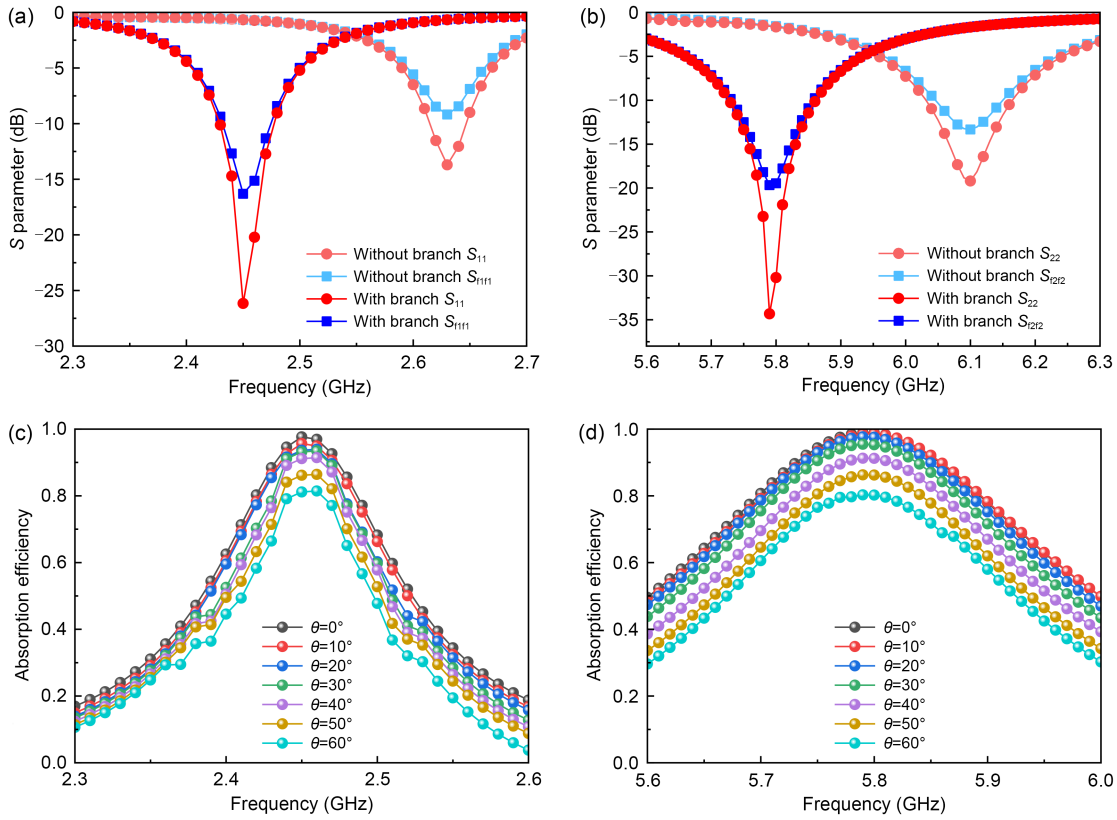

Fig. 8 Reflection coefficient with/without branch and absorption efficiency at different angles of incidence: (a) reflection coefficient at 2.45 GHz; (b) reflection coefficient at 5.8 GHz; (c) absorption efficiency at 2.45 GHz; (d) absorption efficiency at 5.8 GHz. References to color refer to the online version of this figure

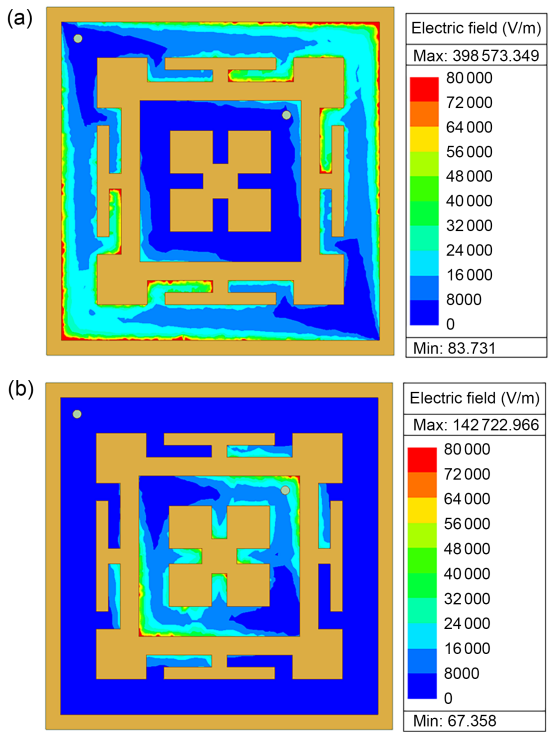

Fig. 9 Electric field distribution of the unit at 2.45 GHz (a) and 5.8 GHz (b)

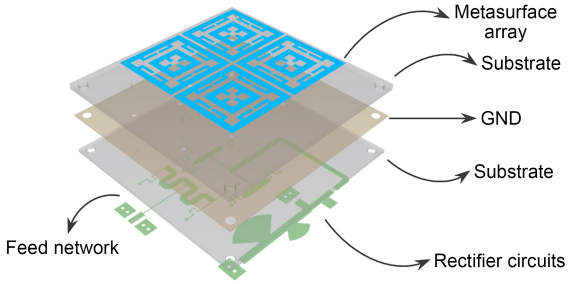

Fig. 10 An exploded diagram of the metasurface array

The simulation results (Fig. 11) show that the array shows good consistency with the resonance characteristics of the unit. The S_{11} values at 2.45 GHz and the S_{22} values at 5.8 GHz are both less than −20 dB. Additionally, the two ports show good isolation characteristics, with S_{21} values less than −20 dB in both operating frequency bands. This ensures minimal interference with information transmission while energy transfer is being conducted. The gain of the metasurface array is measured to be 4.4 dBi at 2.45 GHz and 8.98 dBi at 5.8 GHz, which are lower than the simulation values. The difference between simulated parameters and

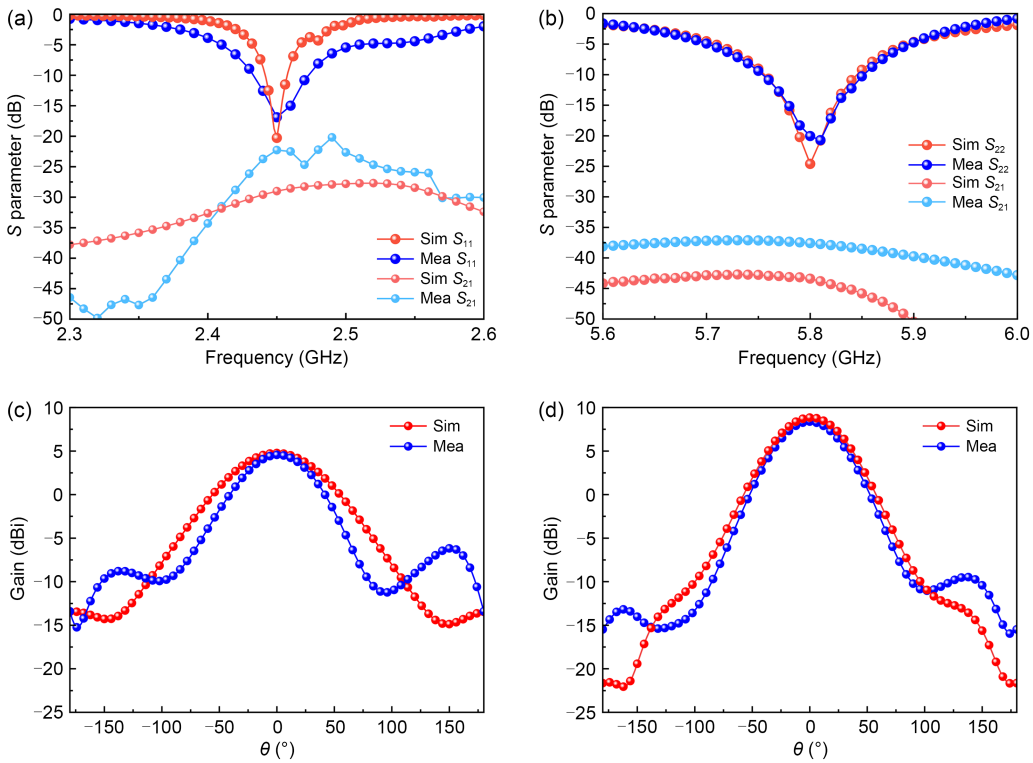

Fig. 11 Reflection coefficients and radiation pattern of the metasurface array: (a) reflection coefficient at 2.45 GHz; (b) reflection coefficient at 5.8 GHz; (c) radiation pattern at 2.45 GHz; (d) radiation pattern at 5.8 GHz. References to color refer to the online version of this figure

experimental parameters is caused by machining errors, but the array still meets the design requirements.

To achieve the conversion of RF energy to DC power, a rectifier circuit integrated with the metasurface is designed to convert the RF energy absorption at the 5.8 GHz frequency band into DC power to directly power the sensors. The structure is shown in Fig. 12a.

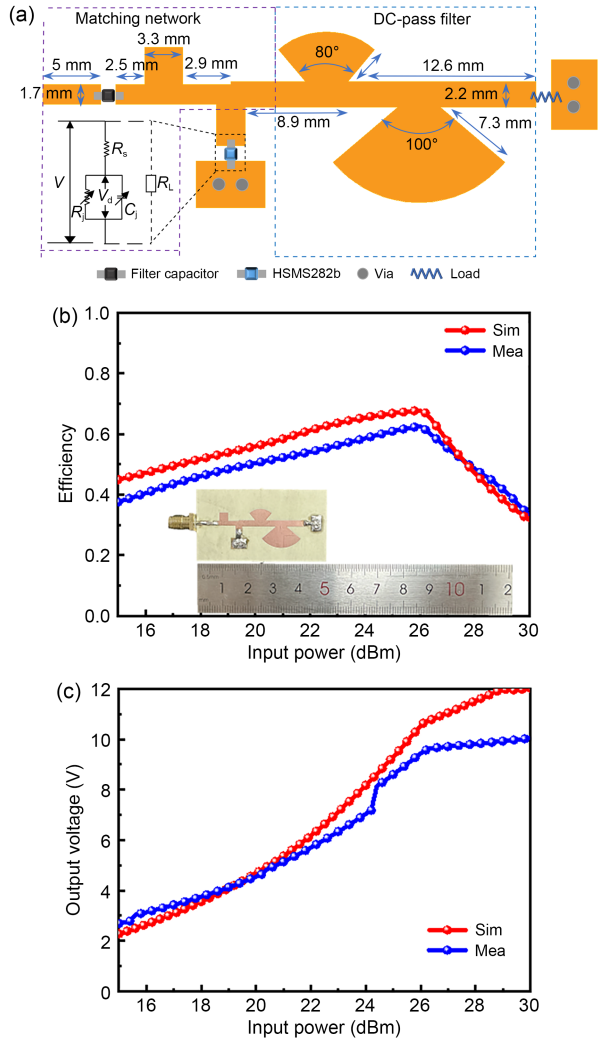

Fig. 12 Structure of the rectifier and relevant results: (a) structure of the rectifier; (b) simulated and experimental parameters of efficiency; (c) simulated and experimental parameters of output voltage. References to color refer to the online version of this figure

To successfully power more sensors, we choose the HSMS282b rectifier diode because of the advantage of adopting a large input power (generally the input power is greater than 20 dBm). Simulations are conducted using Advanced Design System (ADS) 2020. The slight difference between experiment and simulation is due to machining errors. Fig. 12b shows that the curve of rectification efficiency versus input power is obtained through joint simulation at a frequency of 5.8 GHz with a load resistance of 200 Ω. The rectification efficiency remains above 40% for input powers ranging from 12.8 to 28.8 dBm. At 26 dBm, the rectification efficiency reaches its peak value of 67.8%, indicating the high efficiency of the rectifier circuit. Fig. 12c shows the output voltage of the rectifier. The output voltage reaches 10 V when the input power reaches 25.5 dBm, which can achieve the working voltage of most sensors.

2.3 SWIPT system based on the dual-frequency metasurface

To ensure that the proposed metasurface could work successfully in the SWIPT system, we verify that the EM energy received by the metasurface can meet the normal operational requirements of the sensor (Fig. 13a). Considering the space loss, we generate RF energy using the signal generator (AV1141B) and connect it to the amplifier and radiate EM waves through the

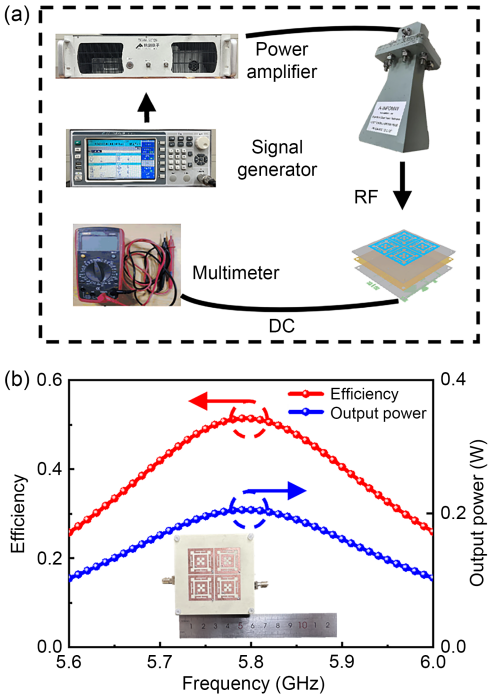

Fig. 13 Measurement of energy reception performance of the metasurface: (a) a schematic view of the experiment; (b) the efficiency and output power of the metasurface. References to color refer to the online version of this figure

horn. The same horn is placed at a distance of 0.5 m and the power received at that distance is measured. We adjust the transmit power until the receiving horn measures 26 dBm of power. We replace the receiving horn with the metasurface in the same position and measure the output power at that time (Fig. 13b). The efficiency is lower than that obtained from simulation calculation because the impedance matching between the metasurface 5.8 GHz port and the input port of the rectifier circuit is poor due to errors in the actual machining process, but it still meets the power demand of the sensor.

To further validate the feasibility of the system, we conduct tests using a height sensor (SPL06) and a Bluetooth module (Fig. 14). The positive and negative output poles of the rectifier circuit are connected to a voltage regulator module to stabilize the output voltage at 3.3 V, which then powers the Bluetooth module and the height sensor. After the height sensor is powered on and functions normally, it transmits data to the Bluetooth module. The Bluetooth module is connected to the metasurface's 2.45 GHz port, and the height information is then transmitted from the metasurface. Finally, the mobile phone receives the height information.

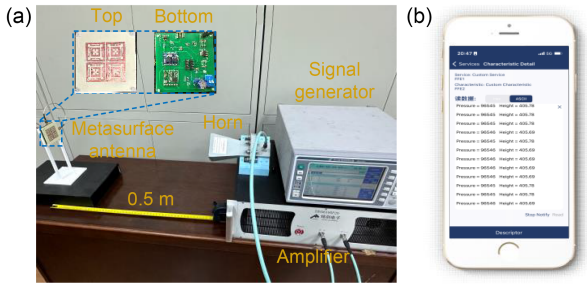

Fig. 14 Measurement of the system (a) and the information received by mobile phone (b)

When the transmitting horn radiates EM waves, the metasurface receives RF energy in the 5.8 GHz frequency band. The rectifier circuit converts RF into DC power, which then powers the sensors. After the sensors operate normally, they transmit information through the 2.45 GHz frequency band. Finally, the mobile phone receives the information sent by the sensors. This system eliminates the need for complex wiring arrangements at the backend and regular battery replacements. Therefore, there is a heavy demand for the power dissipation of the electric appliance in this study because of the gas pressure sensor (10 dBm) and the Bluetooth (9 dBm), and the rectification circuit is designed with the input power considered to be large (26 dBm). The power dissipation of the sensor is low under normal conditions, and there is no need for such a large input power dissipation demand. Metasurfaces are currently being widely applied in new scenarios such as holographic multi-input multi-output (MIMO) process (Gong et al., 2024) and SWIPT. Our design has potential for further expansion in the future, such as using polarization diversity in the SWIPT system to effectively address the looming issue of EM resource scarcity. Additionally, more diversified chip integration can facilitate environmental sensing and adaptive transmission. These advancements offer new approaches for the construction of future smart cities (Liao and Chen, 2022; Shan et al., 2024).

3 Conclusions

In this paper, we present a receiving metasurface designed for the SWIPT system, which uses frequency diversity to achieve the reception of EM energy and the transmission of sensor information. The metasurface achieves efficient absorption of EM energy at 5.8 GHz and radiates sensor information at 2.45 GHz. It offers several advantages such as miniaturization (unit size: $0.16\lambda_0\times0.16\lambda_0\times0.012\lambda_0$), high isolation ($S_{21}<-20$ dB within the operating frequency band), and insensitivity to incident angles (efficiency above 80% within 60°). This design provides a new solution for addressing the power supply issues of multiple sensors in future digital urban development processes.

Contributors

Yicen LI designed the research. Yicen LI and Mingyang CHANG processed the data. Yicen LI drafted the paper. Haixia LIU and Hao XUE helped organize the paper. Hao XUE and Long LI revised and finalized the paper.

Conflict of interest

Long LI is a guest editor of this special issue, and he was not involved with the peer review process of this paper. All the authors declare that they have no conflict of interest.

Data availability

The data that support the findings of this study are available from the corresponding author upon reasonable request.

References

Andrews JG, Buzzi S, Choi W, et al., 2014. What will 5G be? *IEEE J Sel Areas Commun*, 32(6):1065-1082. https://doi.org/10.1109/JSAC.2014.2328098

Bakogianni S, Koulouridis S, 2016. Design of a novel miniature implantable rectenna for in-body medical devices power support. Proc 10th European Conf on Antennas and Propagation, p.1-5. https://doi.org/10.1109/EuCAP.2016.7481970

Chang MY, Li YC, Han JQ, et al., 2024. A compact polarization insensitive rectenna with harmonic suppression for wireless power transfer. *IEEE Antenn Wirel Propag Lett*, 23(1): 119-123. https://doi.org/10.1109/LAWP.2023.3319317

Cheng HW, Yu TC, Luo CH, 2013. Direct current driving impedance matching method for rectenna using medical implant communication service band for wireless battery charging. *IET Microw Antenn Propag*, 7(4):277-282. https://doi.org/10.1049/iet-map.2012.0372

El Badawe M, Ramahi OM, 2018. Efficient metasurface rectenna for electromagnetic wireless power transfer and energy harvesting. *Prog Electromagn Res*, 161:35-40. https://doi.org/10.2528/PIER18011003

Erkmen F, Ramahi OM, 2021. A scalable, dual-polarized absorber surface for electromagnetic energy harvesting and wireless power transfer. *IEEE Trans Microw Theory Techn*, 69(9): 4021-4028. https://doi.org/10.1109/TMTT.2021.3087622

Fang C, Yu FR, Huang T, et al., 2015. A survey of green information-centric networking: research issues and challenges. *IEEE Commun Surv Tut*, 17(3):1455-1472. https://doi.org/10.1109/COMST.2015.2394307

Fante RL, McCormack MT, 1988. Reflection properties of the Salisbury screen. *IEEE Trans Antenn Propag*, 36(10):1443-1454. https://doi.org/10.1109/8.8632

Gao X, Wang XR, Wang WJ, 2023. Polarization-independent dual-band metasurface absorber for wireless power transmission. *J Phys Conf Ser*, 2469(1):012003. https://doi.org/10.1088/1742-6596/2469/1/012003

Gong TR, Gavriilidis P, Ji R, et al., 2024. Holographic MIMO communications: theoretical foundations, enabling technologies, and future directions. *IEEE Commun Surv Tut*, 26(1): 196-257. https://doi.org/10.1109/COMST.2023.3309529

Huang XJ, Wang K, Sun CZ, et al., 2023. A multi-frequency and multi-mode metasurface energy harvester for RF energy harvesting. *Smart Mater Struct*, 32(10):105010. https://doi.org/10.1088/1361-665X/acf424

Langley RJ, Parker EA, 1983. Double-square frequency-selective surfaces and their equivalent circuit. *Electron Lett*, 19(17): 675-677. https://doi.org/10.1049/el:19830460

Lee K, Hong SK, 2020. Rectifying metasurface with high efficiency at low power for 2.45 GHz band. *IEEE Antenn Wirel Propag Lett*, 19(12):2216-2220. https://doi.org/10.1109/LAWP.2020.3027833

Li L, Liu HX, Zhang HY, et al., 2018. Efficient wireless power transfer system integrating with metasurface for biological applications. *IEEE Trans Ind Electron*, 65(4):3230-3239. https://doi.org/10.1109/TIE.2017.2756580

Liao R, Chen L, 2022. An evolutionary note on smart city development in China. *Front Inform Technol Electron Eng*, 23(6): 966-974. https://doi.org/10.1631/FITEE.2100407

Lin W, Ziolkowski RW, 2019. Electrically small Huygens antenna-based fully-integrated wireless power transfer and communication system. *IEEE Access*, 7:39762-39769. https://doi.org/10.1109/ACCESS.2019.2903545

Liu HX, Li YC, Cheng FJ, et al., 2024. Holographic tensor metasurface for simultaneous wireless powers and information transmissions using polarization diversity. *Adv Funct Mater*, 34(2):2307806. https://doi.org/10.1002/adfm.202307806

Lu P, Yang XS, Wang BZ, 2017. A two-channel frequency reconfigurable rectenna for microwave power transmission and data communication. *IEEE Trans Antenn Propag*, 65(12): 6976-6985. https://doi.org/10.1109/TAP.2017.2766450

Mohsan SAH, Qian H, Amjad H, 2023. A comprehensive review of optical wireless power transfer technology. *Front Inform Technol Electron Eng*, 24(6):767-800. https://doi.org/10.1631/FITEE.2100443

Piñuela M, Mitcheson PD, Lucyszyn S, 2013. Ambient RF energy harvesting in urban and semi-urban environments. *IEEE Trans Microw Theory Techn*, 61(7):2715-2726. https://doi.org/10.1109/TMTT.2013.2262687

Shan Z, Shi L, Li B, et al., 2024. Empowering smart city situational awareness via big mobile data. *Front Inform Technol Electron Eng*, 25(2):286-307. https://doi.org/10.1631/FITEE.2300453

Shibata T, Sasaya T, Kawahara N, 2001. Development of in-pipe microrobot using microwave energy transmission. *Electron Commun Jpn (Part II Electron)*, 84(11):1-8. https://doi.org/10.1002/ecjb.1067

Wagih M, Hilton GS, Weddell AS, et al., 2021. Dual-band dual-mode textile antenna/rectenna for simultaneous wireless information and power transfer (SWIPT). *IEEE Trans Antenn Propag*, 69(10):6322-6332. https://doi.org/10.1109/TAP.2021.3070230

Wang CC, Zhang JL, Bai SB, et al., 2022. A harmonic suppression energy collection metasurface insensitive to load and input power for microwave power transmission. *IEEE Trans Microw Theory Techn*, 70(8):4036-4044. https://doi.org/10.1109/TMTT.2022.3182238

Wang X, Han JQ, Li GX, et al., 2023. High-performance cost efficient simultaneous wireless information and power transfers deploying jointly modulated amplifying programmable metasurface. *Nat Commun*, 14(1):6002. https://doi.org/10.1038/s41467-023-41763-z

Xue H, Lu ZQ, Ma XJ, et al., 2024. A reconfigurable metasurface enhancing signal coverage for wireless communication using reduced numbers of p-i-n diodes. *IEEE Trans Microw Theory Techn*, 72(3):1964-1978. https://doi.org/10.1109/TMTT.2023.3311952

Yang XX, Jiang C, Elsherbeni AZ, et al., 2013. A novel compact printed rectenna for data communication systems. *IEEE Trans Antenn Propag*, 61(5):2532-2539. https://doi.org/10.1109/TAP.2013.2244550

Yu F, Yang XX, Zhong HT, et al., 2018. Polarization-insensitive wide-angle-reception metasurface with simplified structure for harvesting electromagnetic energy. *Appl Phys Lett*, 113(12):123903. https://doi.org/10.1063/1.5046927

Zhang XM, Liu HX, Li L, 2017. Tri-band miniaturized wide-angle and polarization-insensitive metasurface for ambient energy harvesting. *Appl Phys Lett*, 111(7):071902. https://doi.org/10.1063/1.4999327

Zhong HT, Yang XX, Tan C, et al., 2016. Triple-band polarization-insensitive and wide-angle metamaterial array for electromagnetic energy harvesting. *Appl Phys Lett*, 109(25): 253904. https://doi.org/10.1063/1.4973282